npj | Quantum Materials

www.nature.com/npjquantmats

ARTICLE OPEN

Check for updates

Coexistence of ferromagnetism, antiferromagnetism, and superconductivity in magnetically anisotropic (Eu,La)$FeAs_2$

Jia Yu[1]✉, Congcong Le[2], Zhiwei Li[3], Lisi Li[1], Tong Liu[4,5], Zengjia Liu[1], Bo Zhang[3], Bing Shen[1], Binbin Ruan[4,5], Zhi'an Ren[4,5]✉ and Meng Wang[1]✉

Materials with exceptional magnetism and superconductivity usually conceive emergent physical phenomena. Here, we investigate the physical properties of the (Eu,La)$FeAs_2$ system with double magnetic sublattices. The parent $EuFeAs_2$ shows anisotropy-associated magnetic behaviors, such as Eu-related moment canting and exchange bias. Through La doping, the magnetic anisotropy is enhanced with ferromagnetism of Eu^{2+} realized in the overdoped region, and a special exchange bias of the superposed ferromagnetic/superconducting loop revealed in $Eu_{0.8}La_{0.2}FeAs_2$. Meanwhile, the Fe-related antiferromagnetism shows unusual robustness against La doping. Theoretical calculation and ^{57}Fe Mössbauer spectroscopy investigation reveal a doping-tunable dual itinerant/localized nature of the Fe-related antiferromagnetism. The coexistence of the Eu-related ferromagnetism, Fe-related robust antiferromagnetism, and superconductivity is further revealed in $Eu_{0.8}La_{0.2}FeAs_2$, providing a platform for further exploration of potential applications and emergent physics. Finally, an electronic phase diagram is established for (Eu,La)$FeAs_2$ with the whole superconducting dome adjacent to the Fe-related antiferromagnetic phase, which is of benefit for seeking underlying clues to high-temperature superconductivity.

npj Quantum Materials (2021)6:63 ; https://doi.org/10.1038/s41535-021-00362-1

INTRODUCTION

Magnetism is believed to play an important role in high-temperature superconducting pairing, e.g., the Fe-related antiferromagnetism (Fe-AFM) in the iron-based superconducting family[1–3]. The competition between superconductivity (SC) and Fe-AFM in the charge-lightly doping region has been widely revealed[4–8], however, the systems with unusual phase diagrams are also worth our concern. Typically, in the 112-type (Ca,La)$FeAs_2$[9], the Fe-AFM exhibits robustness and is abnormally enhanced by La doping in the overdoped region, with SC gradually suppressed[10]. Lately, a series of the homogenous (Eu,La)$FeAs_2$ compounds were discovered[11]. The transport and magnetic measurements suggested a structural transition (110 K), a Fe-related antiferromagnetic (Fe-AF) transition (98 K), and an Eu-AF transition (46 K) for single-crystalline $EuFeAs_2$[12]. A recent Mössbauer spectroscopy investigation on the polycrystalline $EuFeAs_2$ sample confirmed an incommensurate spin-density-wave-type (SDW-type) AFM ordering of Fe^{2+} around 106 K[13]. The transport measurements on the underdoped $Eu_{1-x}La_xFeAs_2$ ($x = 0$–0.15) suggest that the Fe-AFM exists in the studied doping region[11]. Hence, the unusual relationship between Fe-AFM and SC in (Eu,La)$FeAs_2$ is anticipated in a broader doping region, than that of (Ca,La)$FeAs_2$ with lightly-doped samples unavailable.

On the other hand, various Eu-related magnetic properties were revealed in polycrystalline $EuFeAs_2$ under a low magnetic field of 10 Oe, including a spin glass (SG) transition, reentrant magnetic modulation, and moment canting induced by transition metal doping in the Fe site[14,15]. The SG and the moment canting indicate a tunable competition and coexistence of the ferromagnetic and AF interactions between the Eu^{2+} ions, which was proposed to mainly originate in the Ruderman–Kittel–Kasuya–Yosida (RKKY) indirect exchange.

More intriguing is that the coupling between the two magnetic sublattices (see the crystal structure[12] in Fig. 1a) would lead to anisotropic interaction between Eu^{2+} and Fe^{2+} in $EuFeAs_2$. Magnetic systems with anisotropic interactions exhibit various magnetic properties, including sign-reversible exchange bias (EB)[16], spin reorientation (SR)[17], thermal magnetic hysteresis[18], etc. The most studied EB effect is an exchange anisotropy with a shift of the magnetic hysteresis loop along the magnetic-field axis, which was first discovered in oxide-coated cobalt particles with moment compensation in the ferromagnetic/AF interface of Co/CoO[19]. Later, single-phase compounds with double magnetic sublattices have been found to exhibit the EB effect due to the existence of anisotropic interactions[20,21]. One explanation is that when a net moment is induced in one of the sublattices by the anisotropic interaction, a circumstance analogous to the FM/AFM interface generates compensation in between. The moment compensation between FM and SDW-type AFM could also trigger the EB effect in alloys or interfaces[22,23]. However, the EB effect associated with SDW-type AFM in a stoichiometric compound system is rare. (Eu,La)$FeAs_2$ with robust SDW-type AFM and doping-modifiable Eu-related magnetism is a suitable compound system for exploring the EB anisotropy. Furthermore, the interplays of exotic magnetism and SC have shown interesting physics and application prospects in layered or wire-like heterostructures[24–29]. Hence, the (Eu,La)$FeAs_2$ system is worth deeper investigation, not only for the unusual relationship between SDW and SC but also for the underlying physics originating from the interplay between anisotropic magnetism and SC.

[1]Center for Neutron Science and Technology, School of Physics, Sun Yat-Sen University, Guangzhou, China. [2]Max Planck Institute for Chemical Physics of Solids, Dresden, Germany. [3]Key Lab for Magnetism and Magnetic Materials of the Ministry of Education, Lanzhou University, Lanzhou, China. [4]Beijing National Laboratory for Condensed Matter Physics, Institute of Physics, Chinese Academy of Sciences, Beijing, China. [5]School of Physical Sciences, University of Chinese Academy of Sciences, Beijing, China. ✉email: jyu_work@163.com; renzhian@iphy.ac.cn; wangmeng5@mail.sysu.edu.cn

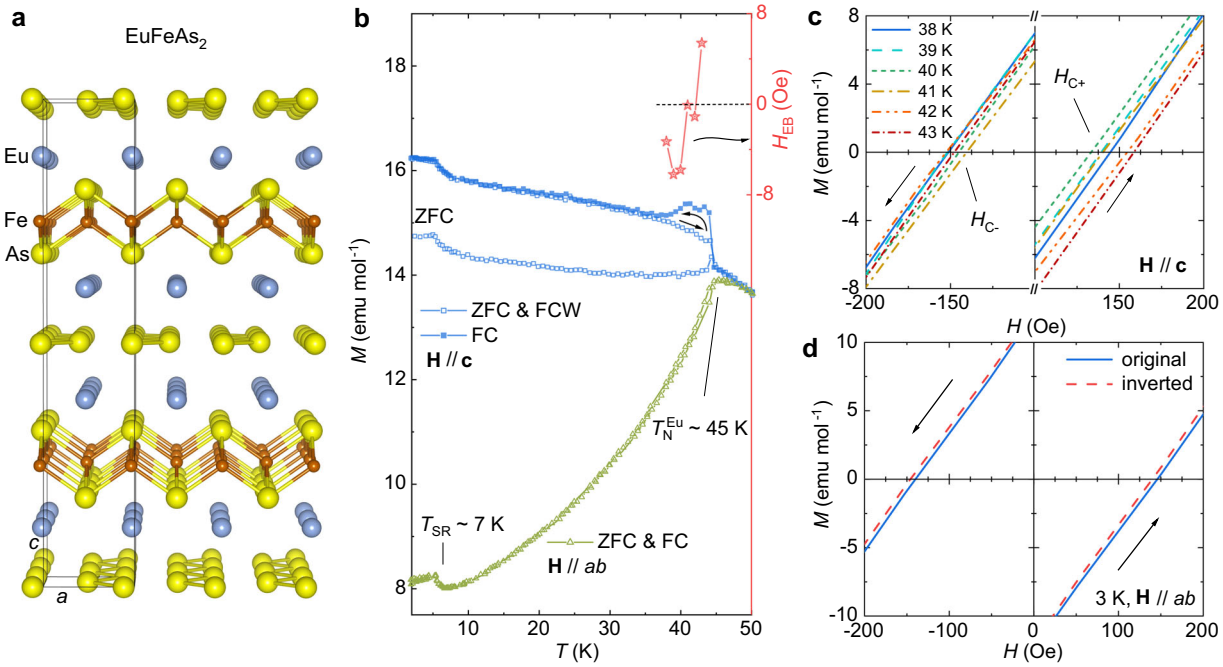

Fig. 1 Crystal structure and magnetic properties of $EuFeAs_2$. **a** Schematic diagram of the crystal structure[12]. **b** Magnetization against temperature under a magnetic field of 100 Oe. **c**, **d** Magnetization against the magnetic field at different temperatures with fields parallel to the *c* direction and the *ab* plane, respectively. The stars to the right axis in (**b**) represent the EB fields of the hysteresis loops in (**c**). The original curve in (**d**), solid, is the obtained *M*–*H* curve. The inverted curve, dashes, is the centrosymmetric one of the original.

In this article, we first illuminate the magnetic anisotropy in the parent $EuFeAs_2$. Then, the La-doping-induced magnetic evolution and the coupling between anisotropic magnetism and SC are studied. The nature of the robust Fe-AFM is discussed and examined in the superconducting state. Finally, a La-doping phase diagram on structure, magnetism, and SC is established.

RESULTS AND DISCUSSION

Magnetic anisotropy in $EuFeAs_2$

The phase transitions of $EuFeAs_2$ are reexamined by heat capacity, high-field magnetization, and single-crystal X-ray diffraction (SXRD) analyses, detailed in Supplementary Fig. 1. Based on the phase transitions, zero-field-cooling (ZFC), field-cooling (FC), and field-cooled-warming (FCW) magnetization measurements were performed on single-crystalline $EuFeAs_2$ under a low magnetic field of 100 Oe below 50 K. The temperature-dependent magnetization (*M*–*T*) curves, depicted in Fig. 1b, exhibit Eu-related AF moment canceling in the *ab* plane and moment canting in the *c* direction below T_N^{Eu} ~45 K. Considering that the RKKY interaction in a conducting system[30] and the anisotropic interaction in an insulating system[31] can both induce net moment, we ascribe the moment canting in $EuFeAs_2$ to the collaboration of the RKKY interaction between Eu^{2+} ions and the anisotropic interaction between Eu^{2+} and Fe^{2+}. An SR-like upturn of the magnetization appears below T_{SR} ~7 K in both directions, corresponding to the reentrant magnetic modulation proposed in the polycrystalline sample[14], while, the SG behavior around 15.5 K is absent in single-crystalline $EuFeAs_2$, even with the magnetic field decreased to 10 Oe, see Supplementary Fig. 2. The hysteresis below T_N^{Eu} for the FC and FCW curves in the *c* direction is reminiscent of the behavior observed in magnetically anisotropic $SmCr_{1-x}Fe_xO_3$, which is attributed to the lower temperature SR[32]. Though the temperature interval of the hysteresis in $EuFeAs_2$ is well above T_{SR}, the hysteresis still implies a metastable spin state probably fixed by the magnetic anisotropy.

The net moment of Eu^{2+} encourages us to explore the EB anisotropy in undoped $EuFeAs_2$. The magnetization versus magnetic field (*M*–*H*) is studied at different temperatures in the thermal-hysteresis interval with magnetic fields parallel to the *c* direction, shown in Fig. 1c (full curves presented in Supplementary Fig. 2). A magnetic hysteresis behavior appears in the *M*–*H* curves, with EB discernible from the comparison between the coercivities H_{C+} and H_{C-}. The EB fields, defined as

$$H_{EB} = (H_{C+} + H_{C-})/2, \quad (1)$$

are summarized in Fig. 1b. The non-monotonic temperature dependence of H_{EB}, is similar to the oscillation behavior associated with incommensurate SDW in the (100)Cr/$Ni_{81}Fe_{19}$ bilayers[23]. We ascribe this EB behavior in $EuFeAs_2$ to the anisotropic interaction between Eu^{2+} and Fe^{2+}. Besides, a sign reversal of EB occurs in the thermal hysteresis interval, which may be related to the metastable spin state. We also performed a magnetization measurement on $EuFeAs_2$ with **H**//*ab* at 3 K, as shown in Fig. 1d. Similar to the scenario of **H**//**c**, a weak EB is observed for **H**//*ab* below T_{SR}, as seen from the comparison between the original and inverted curves. Thus, a weak net moment and a moment compensation emerge in the *ab* plane as well. The FCW measurement below T_{SR} with **H**//*ab* has also been conducted, while, the magnetization curve basically overlaps with the FC and ZFC curves due to the measurement error of the physical property measurement system (PPMS).

In a word, the single-crystalline $EuFeAs_2$ shows various magnetic properties, mainly associated with magnetic anisotropy. The EB behaviors related to SDW-type AFM in a stoichiometric compound system enrich the EB effect and the platforms for investigating the mechanism of EB anisotropy.

La-doping effects in $Eu_{0.79}La_{0.21}FeAs_2$

La-doping effects are investigated in overdoped single-crystalline $Eu_{0.79}La_{0.21}FeAs_2$, of which the doping level is determined by an energy-dispersive X-ray spectroscopy (EDXS) analysis, detailed in Supplementary Fig. 5. The electrical transport measurement was

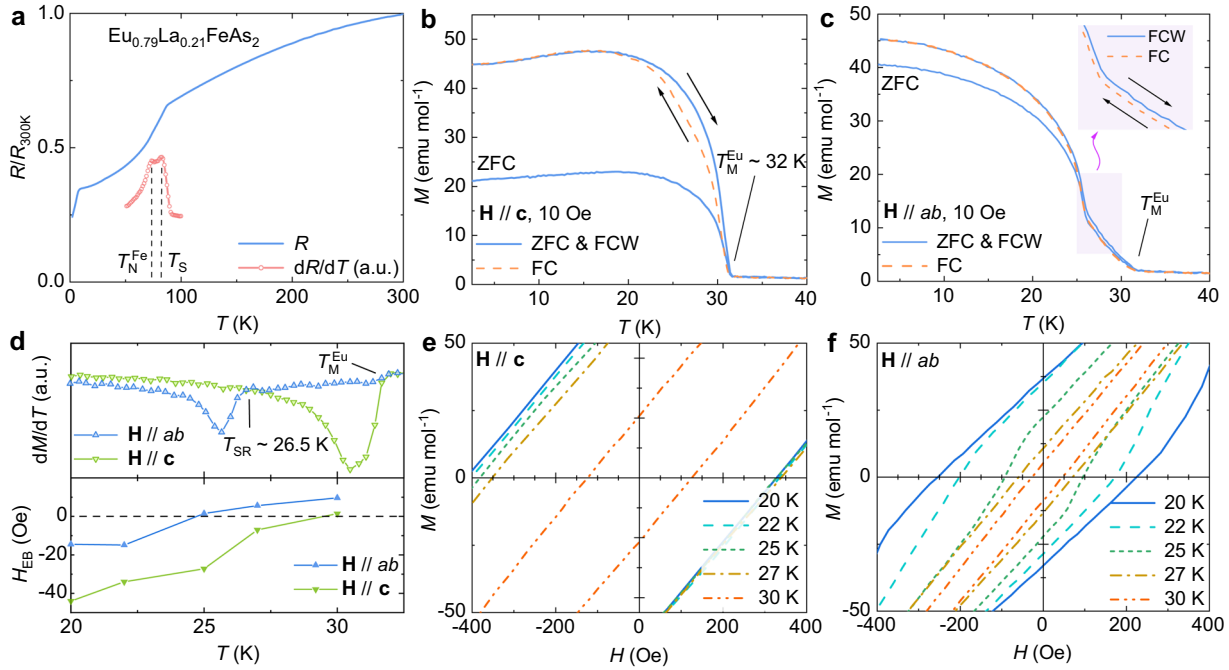

Fig. 2 Physical properties of $Eu_{0.79}La_{0.21}FeAs_2$. a Normalized in-plane resistivity against temperature with part of the first derivation curve. **b**, **c** Magnetization against temperature with magnetic fields parallel to different directions. **d** First derivation of the *M*–*T* curves (10 Oe) and the EB fields in different directions. **e**, **f** Magnetization against the field in different directions. The inset in **c** is the enlarged view of the thermal hysteresis of the FC and FCW curves in the shadow area.

carried out to check the structural and Fe-AF transitions in this overdoped sample, as demonstrated in Fig. 2a. The resistivity curve exhibits an anomaly around 80 K, similar to that around 100 K in the parent $EuFeAs_2$[12]. According to the phase transitions of the parent $EuFeAs_2$ (see Supplementary Fig. 1), the derivation of the *R*–*T* curve indicates that the structural and Fe-AF transitions are suppressed to T_S ~82 K and T_N^{Fe} ~73 K, respectively. The slight resistivity decreasing below 8 K indicates that SC is greatly destroyed, despite the remaining of the robust Fe-AFM.

The *M*–*T* curves, demonstrated in Fig. 2b, c, exhibit a dramatic ferromagnetic transition at T_M^{Eu} ~32 K for both directions, and an SR-like transition at T_{SR} ~26.5 K (determined from the derivation of *M*–*T* in Fig. 2d) in the *ab* plane. The magnetic susceptibility can be suppressed by larger fields (not demonstrated), manifesting the canted AF nature of the Eu-FM with field-modifiable competing ferromagnetic and AF interactions. Thermal hysteresis of the FC and FCW processes exists in both directions below T_M^{Eu}, which is probably associated with magnetic anisotropy. No superconducting diamagnetic behavior appears below 8 K.

For comparison, a series of Pr-doped (Eu,Pr)$FeAs_2$ samples are synthesized, of which Pr doping introduces equal electrons but with less magnetic dilution comparing to equally La doping. All the Pr-doped samples exhibit weak moment canting behaviors, even in the overdoped region, detailed in Supplementary Fig. 8. Thus, the emergence of the stronger FM in (Eu,La)$FeAs_2$ can be mainly attributed to the La-doping-induced magnetic dilution effect, rather than simply the doping-introduced extra electrons modifying the RKKY interaction. We consider the origin of the net moment in $Eu_{0.79}La_{0.21}FeAs_2$ the same as that in the parent phase discussed above. Then, there are two possible ways to trigger the magnetic dilution effect on enhancing the magnetic anisotropy and generate FM: (1) The anisotropic exchange between Eu^{2+} and Fe^{2+} is adjusted by introducing nonmagnetic La^{3+}, which leads to the change of the ferromagnetic-AF competition, similar to the dilution effect in (Sm,La)FeO_3[33]. (2) The nonmagnetic La^{3+} will not participate the RKKY interaction, which results in the doubling of the interaction distance between the Eu^{2+} moments beside the La^{3+} ion and might change the proportion of the ferromagnetic term of the RKKY interaction.

To further illuminate the La-doping effect on the exchange anisotropy, isothermal magnetization measurements were performed at different temperatures in the thermal-hysteresis interval, as shown in Fig. 2e, f (full curves seen in Supplementary Fig. 3). The areas of the magnetic loops are reasonably larger than those of the parent $EuFeAs_2$. EB emerges in both the *ab* and *c* directions, with a longitudinal shift along the magnetization axis. The EB fields for different temperatures are summarized in Fig. 2d. The increased H_{EB}s from those of the parent $EuFeAs_2$, and the longitudinal shift of the loop support the enhancement of the magnetic anisotropy in $Eu_{0.79}La_{0.21}FeAs_2$. A sign reversal of EB occurs below T_M^{Eu} for **H**//**c**, while, below T_{SR} for **H**//*ab*.

It is worth mentioning that higher magnetic fields are needed to reverse the partially frozen moment at a lower temperature. Hence, a lower magnetic field only results in *M*–*H* curves with a loop area close to zero at a low temperature, shown in Supplementary Fig. 3. The almost linear *M*–*H* curve shows an upward shift with bias in the field direction, which is similar to that observed in (Sm,La)FeO_3[33]. The upward shift can be ascribed to the pinning between the partially frozen magnetic moment and the reversible magnetic moment.

Briefly, La doping greatly affects the competing balance between the ferromagnetic and AF interactions of the Eu^{2+} sublattice and enhances the magnetic anisotropy in $Eu_{1-x}La_xFeAs_2$.

The interplay of the anisotropic magnetism and SC

To explore the interplay of the anisotropic magnetism and SC, an overdoped sample with a sharper superconducting transition is requisite. Here, a series of $Eu_{1-x}La_xFeAs_2$ (x = 0.2, 0.25, and 0.3) polycrystalline samples are prepared and investigated. The chemical phase and quality of the samples are examined by powder X-ray diffraction (PXRD), detailed in Supplementary Fig. 6. For these polycrystalline samples, we use the nominal doping levels to represent the La-doping contents. From the resistivity curves depicted in Fig. 3a, the anomaly related to the structural

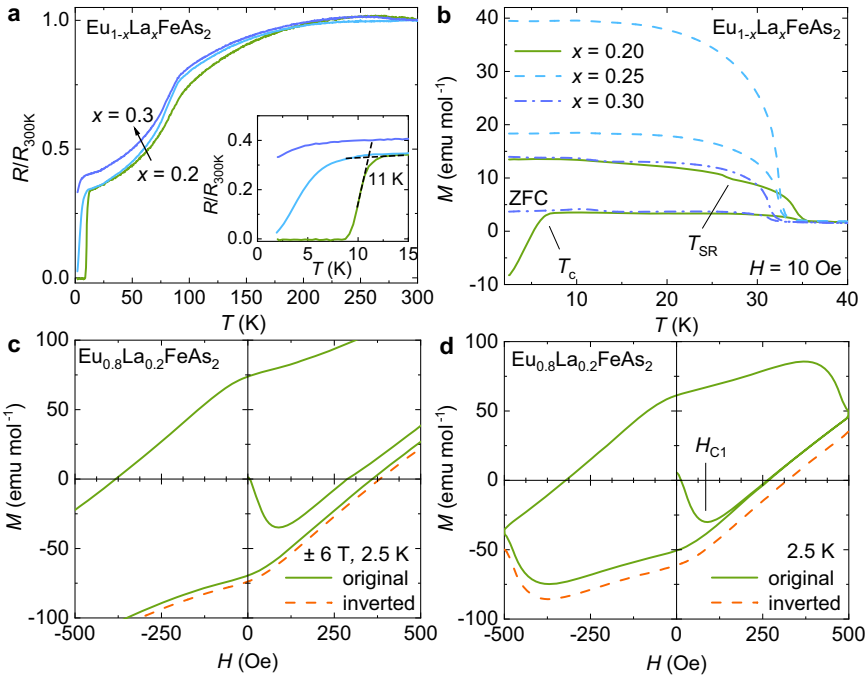

Fig. 3 Physical properties of overdoped $Eu_{1-x}La_xFeAs_2$. a, **b** Normalized resistivity and magnetization against temperature, respectively. **c**, **d** Magnetization against the field for different field intervals of −6 to 6 T and −500 to 500 Oe, respectively, obtained at 2.5 K. The inset in **a** is a close view of the superconducting transition. Parts of the inverted *M*–*H* curves, dashes in **c** and **d**, are for comparison with the original ones.

and Fe-AF transitions remains in these overdoped samples. As magnified in the inset of Fig. 3a, a sharp superconducting transition at T_c ~11 K is realized for $x = 0.2$, which is suppressed with further doping. Zero resistivity is realized below T_{zero} ~8.5 K for $Eu_{0.8}La_{0.2}FeAs_2$. Hence, $Eu_{0.8}La_{0.2}FeAs_2$ is the expected superconducting compound.

Temperature dependences of magnetization were measured for these overdoped samples, as depicted in Fig. 3b. Eu-related ferromagnetic transition occurs in all the samples, different from the AF behavior of the compounds with $x \leq 0.15$[11]. The magnetization increases from $x = 0.2$ to 0.25, indicating an enhancement of the ferromagnetic interaction. Then, it is suppressed by further La doping, implying an excessive magnetic dilution. Meanwhile, the SR-like behavior gradually disappears in these overdoped samples. A diamagnetic transition appears at 7 K for $Eu_{0.8}La_{0.2}FeAs_2$ in the ZFC process, with a superconducting volume fraction estimated to be 0.15–0.2 at 2.5 K. The broad superconducting transition for $Eu_{0.75}La_{0.25}FeAs_2$ in the *R*–*T* curve disappears in the *M*–*T* curve, which probably originates in the slight inhomogeneity nature for the polycrystalline sample and/or the filamentary SC.

ZFC isothermal magnetization was studied at 2.5 K for $Eu_{0.8}La_{0.2}FeAs_2$. The magnetic hysteresis loop obtained in a large field interval of −6 to 6 T is enlarged in Fig. 3c. The full and less-enlarged *M*–*H* curves can be seen in Supplementary Fig. 4. The misalignment of the first quarter (0 → 6 T) and the last two quarters (−6 → 6 T) of the loop are due to the superposition of the superconducting and ferromagnetic loops. The superposed loop exhibits an EB behavior with H_{EB} ~−19 Oe, as seen from the comparison between the original and inverted curves.

As mentioned above, a lower magnetic field results in bias curves with a loop area close to zero at lower temperatures. Thus, to eliminate the component of the ferromagnetic loop, the isothermal magnetization in a smaller field interval is studied, as shown in Fig. 3d. The first quarter and the fifth quarter of the loop coincide fast when passing the lower critical field H_{C1}, indicating that the superconducting loop is no longer superposed on the ferromagnetic loop. Meanwhile, an enhanced EB with H_{EB} ~−54 Oe is obtained.

In short, combining of the anisotropic magnetism and SC leads to an EB behavior of the superposed magnetic and superconducting loop for $Eu_{0.8}La_{0.2}FeAs_2$. This compound with the interplay between SC and anisotropic magnetism may serve as a prototype for application exploration. Also, seeking emergent physical phenomena from the interplay between multiple magnetic and superconducting orders is promising in this material.

Nature of the Fe-AFM, and the FM/AFM/SC coexisting state

To understand the nature of the robust Fe-AFM, we performed a density functional theory (DFT) calculation on the band structure of $EuFeAs_2$. Without considering the magnetic order of Eu^{2+}, seen in Fig. 4a, the band structures near the Fermi level are mainly attributed to the Fe-3*d* orbitals, of which the t_{2g} orbitals contribute to the hole pockets at the Γ point and the electron pockets at the M point, similar to the band structure of LaFeAsO[34]. Following the magnetic structure of $EuFe_2As_2$[35], an assumed A-type AF order of Eu^{2+} was considered in the calculation, as seen in Fig. 4b. The band structures near the Fermi level barely changes, and the Eu-4*f* orbitals are below the Fermi level. Figure 4c shows the Fermi surface (FS) of $EuFeAs_2$ with Fermi level $E_f = 0$ lying at the charge neutral point. Similar to that in the Ca112 system[36], a reasonable FS nesting exists between the electron pockets at the M site and the hole pockets at the Γ point, suggesting the appropriate origin of the SDW-type AFM in $EuFeAs_2$. In order to further explore the influence of electron doping, we artificially raise the Fermi level to examine the changes of the FS. The FSs with Fermi level $E_f = 30$ and 50 meV (corresponding to 0.07 and 0.12 electron doping per Fe) are displayed in Fig. 4d, e, respectively, where the FS nesting is gradually weakened by electron doping but always exists.

The SDW-type Fe-AFM of $(Eu,La)FeAs_2$ in the underdoping region can be explained by the FS nesting, despite the La-doping induced structural transformation[11,12], as discussed in

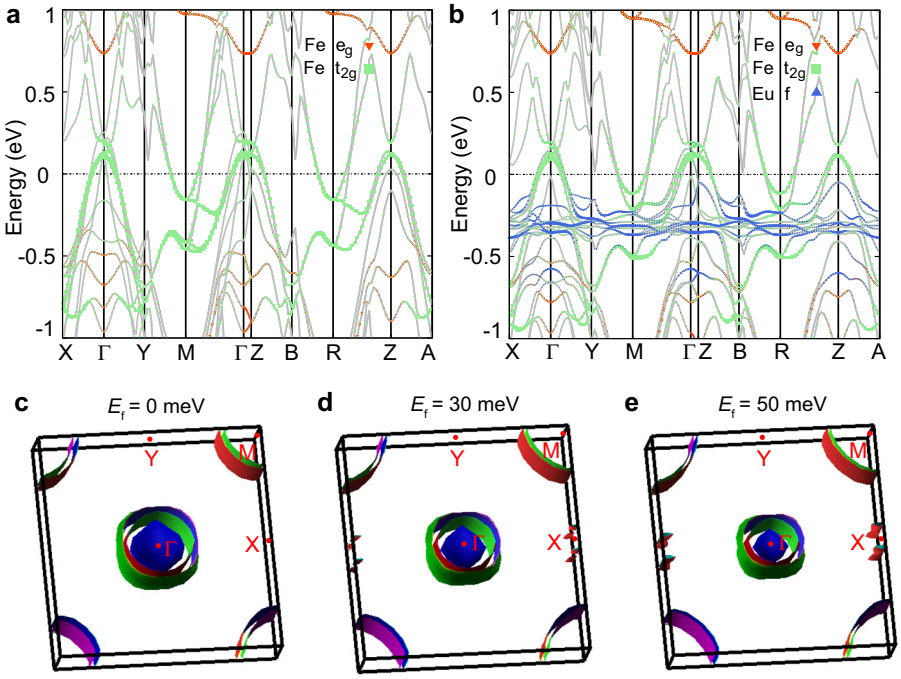

Fig. 4 DFT calculations on $EuFeAs_2$. a, b Band structures without and with A-type AF order at the Eu^{2+} site, respectively, where the areas of the symbols represent the weights of the Fe *d*- and Eu *f*-orbitals. **c**–**e** Fermi surfaces with corresponding Fermi levels $E_f = 0$, 30, and 50 meV, respectively.

Supplementary Fig. 10. Whereas the FS nesting is gradually destroyed with electron doping exceeding 0.12 (Supplementary Fig. 11). A dual itinerant and localized nature is proposed for the Fe-AFM in $Ca_{0.73}La_{0.27}FeAs_2$[36] and other iron-based systems[37]. Given that the ordered magnetic moment of Fe^{2+} in $EuFeAs_2$ ($0.78\mu_B$)[13] is relatively larger than many other iron-pnictide parents[38–40], we consider that the Fe-AFM in this Eu112 system is also dual-natured. Thus, with the FS nesting in (Eu,La)$FeAs_2$ weakened by La doping, the Fe-AFM in the overdoped region is probably contributed increasingly by the local superexchange interaction.

To further reveal the nature of the Fe-AFM in the overdoped area, as well as to check if it survives in the superconducting state, we performed a ^{57}Fe Mössbauer spectroscopy investigation on the superconducting $Eu_{0.8}La_{0.2}FeAs_2$ polycrystalline sample. The fit of the ^{57}Fe Mössbauer spectrum obtained at 300 K, detailed in Supplementary Fig. 12, reveals a nearly single iron-containing phase. The fitted isomer shift (IS) and quadrupole splitting (QS) are 0.432(1) and 0.157(4) mm s^{-1}, respectively, which are close to the corresponding values for the parent $EuFeAs_2$ and the Ni-doped $EuFe_{0.97}Ni_{0.03}As_2$[13].

The spectrum collected at 6 K ($<T_c$), as shown in Fig. 5a, is similar to that of the undoped $EuFeAs_2$[13] in the form of a broadened, asymmetric, six-line Zeeman pattern, which can be explained by the distribution of hyperfine magnetic field due to the SDW-type AF order. To fit the spectrum of 6 K in the main text, we follow the procedure reported in ref. [41]. In general, the hyperfine magnetic field of the spin-density-wave order can be expressed as

$$H(qX) = \sum_{n=1}^{N} h_{2n-1}\sin[(2n-1)qX], \tag{2}$$

where h_{2n-1} denote the amplitudes of subsequent harmonics, q stands for the wavenumber of the SDW, and X denotes the relative position of the resonant nucleus along the propagation direction of the stationary SDW. The root-mean-square value of the hyperfine magnetic field $\sqrt{\langle H^2\rangle}$ can be obtained as

$$\sqrt{\langle H^2\rangle} = \sqrt{\frac{1}{2}\sum_{n=1}^{N} h_{2n-1}^2}, \tag{3}$$

which is proportional to the ordered magnetic moment μ_{Fe} carried by the Fe atoms. It is generally accepted that the magnetic moment is approximately proportional to the measured hyperfine magnetic field. The obtained hyperfine parameters are listed in Supplementary Table 1, and the resulting SDW shape and the corresponding hyperfine field distribution are shown in Fig. 5b, c, respectively. The magnetic moment is determined to be 0.84(1) μ_B by using the same proportionality constant of $a = 63$ kOe μ_B^{-1} as was used for the calculation of the magnetic moment of the parent compound $EuFeAs_2$[13]. The ordered magnetic moment is much larger than those of other iron-based superconducting samples with suppressed Fe-AFM[42–44]. Another interesting result is that the SDW shape is almost rectangular rather than quasi-triangular as found in most iron-based superconductors[13,42,43]. The rectangular SDW shape at a low temperature has been observed in some of the parent compounds with relatively large magnetic moments and less pronounced itinerant character[41]. Besides, the ratio of the third and first amplitudes h_3/h_1 ~0.36, which outclasses the range of 10^{-3}–10^{-2} expected from the itinerant-electron model[45–47], implies that the Fe-AFM in $Eu_{0.8}La_{0.2}FeAs_2$ cannot be accurately described merely by the itinerant picture. All these unusual Mössbauer spectroscopy results put our sample closer to the localized-AFM nature with the itinerant character of the magnetic order less prominent. Also, the magnetic moment is enhanced from that of the parent $EuFeAs_2$[13], which is in agreement with the increasing prominence of the local superexchange interaction suggested by the DFT calculation.

On the other hand, the Mössbauer spectrum obtained at 6 K manifests a microscopic coexistence of the Fe-AFM and SC. Given the relatively small superconducting volume fraction of $Eu_{0.8}La_{0.2}$-$FeAs_2$, the robust Fe-AFM remains in the superconducting state

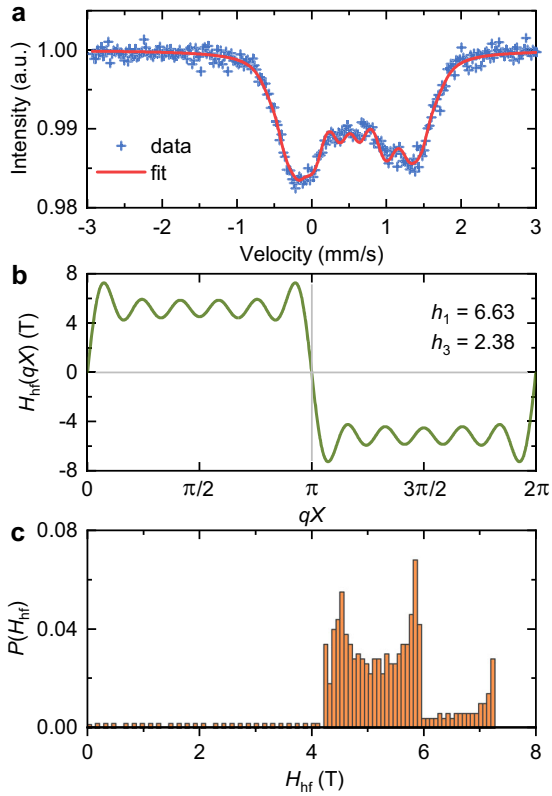

Fig. 5 ^{57}Fe Mössbauer spectroscopy analysis on $Eu_{0.8}La_{0.2}FeAs_2$. **a** The spectrum (blue crosses) obtained at 6 K and the fit (red solid line) with the SDW model detailed in the main text. **b** the SDW shape, and **c** the resulting hyperfine field distribution.

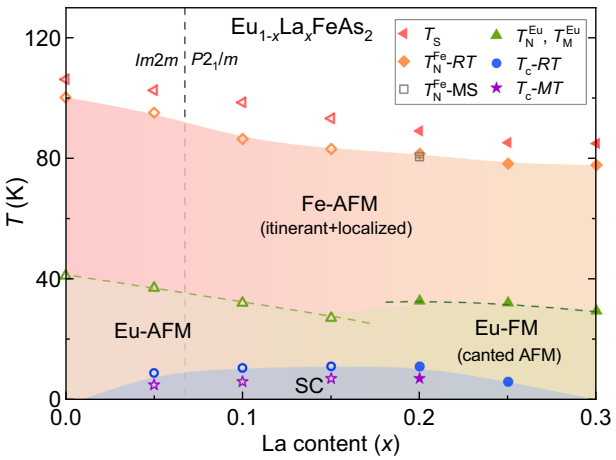

Fig. 6 Electronic phase diagram of $Eu_{1-x}La_xFeAs_2$. The structural, Fe-AF, Eu-related magnetic, and superconducting transition temperatures as functions of the nominal La doping content x for the polycrystalline samples. The open symbols for $x \le 0.15$ represent the data extracted from our previous work[11], and the solid symbols for $x \ge 0.15$ the data obtained in the present work. The structural transition temperatures (T_S), the Fe-AF transition temperatures $\left(T_N^{Fe} - RT\right)$, and the superconducting transition temperatures ($T_c - RT$) are obtained from the transport measurements. The Fe-AF transition temperature $\left(T_N^{Fe} - \mathrm{MS}\right)$ for $x = 0.2$ is obtained from the Mössbauer spectroscopy investigation, where the error bar represents the s.e.m. The Eu-magnetic transition temperatures $\left(T_N^{Eu}\text{ and }T_M^{Eu}\right)$ and the diamagnetic transition temperatures ($T_c - MT$) are obtained from the magnetization measurements.

probably with a cost of suppression on SC. Anyhow, $Eu_{0.8}La_{0.2}FeAs_2$ exhibits a microscopic coexistence of Eu-FM, Fe-AFM, and SC at low temperatures, similar to the Co-doped $EuFe_2As_2$ system[30,44].

Finally, combining the results above and the data we previously reported on the lightly-doped compounds[11], a La-doping electronic phase diagram on structure, magnetism, and SC for $Eu_{1-x}La_xFeAs_2$ is assembled in Fig. 6. All the values of the transition temperatures included in the phase diagram are listed in Supplementary Table 2. The La-doping-induced structural transformation occurs around x ~0.05–0.1 (detailed in Supplementary Fig. 7), which barely impacts the property evolution. The structural and Fe-AF transition temperatures are obtained from the derivation of the R–T curves, see Supplementary Fig. 9. The Fe-AF transition temperature of $Eu_{0.8}La_{0.2}FeAs_2$ obtained from the Mössbauer spectroscopy investigation (Supplementary Fig. 13) is included for comparison, which manifests the reliability of the Fe-AF transition temperatures extracted from the R–T data. Both the structural and Fe-AF transitions are slightly suppressed by La doping but robustly remain. The slight suppression of the Fe-AFM by La doping in $(Eu,La)FeAs_2$ is likely due to the weakened FS nesting, which is contrary to the overdoped $(Ca,La)FeAs_2$ with stronger FS nesting and doping-enhanced Fe-AFM[10,36]. Consequently, the Fe-AFM phase with doping-adjustable dual nature is unusually adjacent to the whole superconducting dome. The robustness of the Fe-AFM is universal for electron doping in the Eu site, see the phase diagram of $(Eu,Pr)FeAs_2$ in Supplementary Fig. 8. On the other hand, the Eu^{2+} magnetic moments in $EuFeAs_2$ start to order below 45 K with a weak moment canting, leading to the coexistence of the Fe^{2+} and Eu^{2+} magnetic orders. The moment canting of the Eu^{2+} sublattice is tunable by La doping, with the AF transition temperature suppressed with doping level increasing in the underdoped region. FM originating from the canted AF order of the Eu^{2+} sublattice is realized for $x \ge 0.2$, with a higher ordering temperature than that of the AF transition temperature for $x = 0.15$, indicating the domination of the ferromagnetic interaction. With temperature further dropping, a superconducting dome is obtained by La doping. Under the dome, the superconducting order coexists with the Fe- and Eu-magnetic orders.

In summary, we systematically investigated the electrical and magnetic properties of the 112-type $(Eu,La)FeAs_2$. Due to the magnetic anisotropy, various exceptional magnetic phenomena are discovered in the parent $EuFeAs_2$. Nonmagnetic La substitution modifies the balance of the ferromagnetic-AF competition and enhances the magnetic anisotropy. Several related physical phenomena are further revealed, including the EB effect of the superposed ferromagnetic/superconducting loop; the robustness of the Fe-AFM with doping-adjustable dominance of the dual itinerant and localized nature; and the coexisting state of Eu-FM, Fe-AFM, and SC. We call for further theoretical explanations for the SDW-associated magnetic exchange anisotropy. The incorporation of superconducting electrons and anisotropic spin states may trigger explorations of applications in electronics and spintronics, for example, in the cross-control field. Experimental investigations of the underlying physical phenomena in the FM/AFM/SC coexisting state are promising, given the coexistence of the multiple orders and the strong couplings. Most importantly, SC adjacent to the Fe-AFM with doping-adjustable itinerant/localized characters may host different threads to the nature of high-temperature SC in different doping regions.

METHODS

Sample preparation

Single crystals of $EuFeAs_2$ and $Eu_{0.79}La_{0.21}FeAs_2$ were grown from a CsCl flux. A mixture of elementary Eu/La, Fe, and As in ratio of 1:1:4 (or 2:1:6)

with 10- to 20-fold of dehydrated CsCl was sealed in a vacuum quartz tube, heated slowly to 800 °C, and held for 2 weeks before quenching. Polycrystalline $Eu_{1-x}La_xFeAs_2$ (x = 0.2, 0.25, and 0.3) samples were synthesized following our previous work[11]. The reaction temperature in the last step was modulated to 850 °C to improve the La-doping homogeneity in the overdoped samples.

Phase and property characterization

The SXRD experiments were carried out on a Single-crystal X-ray Diffractometer (Bruker). The PXRD patterns were collected on a Powder X-ray Diffractometer (PAN-analytical). The EDXS experiment was performed using a Scanning Electron Microscope (SEM) equipped with an energy dispersive X-ray spectrometer. Electrical transport, heat capacity, and magnetic measurements were conducted on a PPMS and a magnetic property measurement system (MPMS) (Quantum Design).

Transmission ^{57}Fe Mössbauer spectra were recorded by using a conventional spectrometer working in constant acceleration mode. A 50 mCi of ^{57}Co embedded in an Rh matrix moving at room temperature was used as the γ-ray source. The absorber was prepared with a surface density of ~8 mg cm^{-2} natural iron. The drive velocity was calibrated with sodium nitroprusside at room temperature and all the ISs quoted in this work are relative to that of the α-Fe.

Theoretical calculations

Theoretical calculations were performed using the DFT as implemented in the Vienna ab initio simulation package code[48–50]. The generalized-gradient approximation for the exchange-correlation functional was used. The cutoff energy was set to be 400 eV for expanding the wave functions into a plane-wave basis. In the calculation, the BZ was sampled in the k space within Monkhorst–Pack scheme[51].

DATA AVAILABILITY

The data that support the findings of this study are available from the corresponding authors upon reasonable request.

Received: 12 January 2021; Accepted: 10 June 2021;
Published online: 25 June 2021

REFERENCES

1. Kamihara, Y., Watanabe, T., Hirano, M. & Hosono, H. Iron-based Layered Superconductor La[$O_{1-x}F_x$]FeAs (x = 0.05-0.12) with T_c = 26 K. *J. Am. Chem. Soc.* **130**, 3296–3297 (2008).
2. Fernandes, R. M. et al. Unconventional pairing in the iron arsenide superconductors. *Phys. Rev. B* **81**, 140501 (2010).
3. Scalapino, D. J. A common thread: the pairing interaction for unconventional superconductors. *Rev. Mod. Phys.* **84**, 1383–1417 (2012).
4. Dong, J. et al. Competing orders and spin-density-wave instability in La($O_{1-x}F_x$)FeAs. *Europhys. Lett.* **83**, 27006 (2008).
5. Huang, Q. et al. Doping evolution of antiferromagnetic order and structural distortion in $LaFeAsO_{1-x}F_x$. *Phys. Rev. B* **78**, 054529 (2008).
6. Drew, A. J. et al. Coexistence of static magnetism and superconductivity in $SmFeAsO_{1-x}F_x$ as revealed by muon spin rotation. *Nat. Mater.* **8**, 310–314 (2009).
7. Chen, H. et al. Coexistence of the spin-density wave and superconductivity in $Ba_{1-x}K_xFe_2As_2$. *Europhys. Lett.* **85**, 17006 (2009).
8. Oka, T. et al. Antiferromagnetic spin fluctuations above the dome-shaped and full-gap superconducting states of $LaFeAsO_{1-x}F_x$ revealed by ^{75}As-nuclear quadrupole resonance. *Phys. Rev. Lett.* **108**, 047001 (2012).
9. Katayama, N. et al. Superconductivity in $Ca_{1-x}La_xFeAs_2$: a novel 112-type iron pnictide with arsenic zigzag bonds. *J. Phys. Soc. Jpn.* **82**, 123702 (2013).
10. Kawasaki, S. et al. Doping-enhanced antiferromagnetism in $Ca_{1-x}La_xFeAs_2$. *Phys. Rev. B* **92**, 180508 (2015).
11. Yu, J. et al. Discovery of a novel 112-type iron-pnictide and La-doping induced superconductivity in $Eu_{1-x}La_xFeAs_2$ (x = 0-0.15). *Sci. Bull.* **62**, 218–221 (2017).
12. Yu, J. et al. Single crystal growth and characterization of the 112-type iron-pnictide $EuFeAs_2$. *Acta Phys. Sin.* **67**, 207403 (2018).
13. Albedah, M. A., Stadnik, Z. M., Fedoryk, O., Liu, Y. B. & Cao, G. H. Magnetic properties of $EuFeAs_2$ and the 14 K superconductor $EuFe_{0.97}Ni_{0.03}As_2$. *J. Magn. Magn. Mater.* **503**, 166603 (2020).
14. Liu, Y. B., Liu, Y., Jiao, W. H., Ren, Z. & Cao, G. H. Magnetism and superconductivity in $Eu(Fe_{1-x}Ni_x)As_2$ (x = 0, 0.04). *Sci. China Phys. Mech.* **61**, 127405 (2018).
15. Yu, J. et al. Co-doping effects on magnetism and superconductivity in the 112-type $EuFeAs_2$ system. *Sci. China Phys. Mech. Astron.* **64**, 267411 (2021).
16. Fita, I., Wisniewski, A., Puzniak, R., Markovich, V. & Gorodetsky, G. Exchange-bias reversal in magnetically compensated $ErFeO_3$ single crystal. *Phys. Rev. B* **93**, 184432 (2016).
17. Cooke, A. H., Martin, D. M. & Wells, M. R. Magnetic interactions in gadolinium orthochromite, $GdCrO_3$. *J. Phys. C* **7**, 3133–3144 (1974).
18. Tsymbal, L. T., Bazaliy, Y. B., Kakazei, G. N. & Vasiliev, S. V. Mechanisms of magnetic and temperature hysteresis in $ErFeO_3$ and $TmFeO_3$ single crystals. *J. Appl. Phys.* **108**, 083906 (2010).
19. Meiklejohn, W. H. & Bean, C. P. New magnetic anisotropy. *Phys. Rev.* **102**, 1413–1414 (1956).
20. Singh, R. P., Tomy, C. V. & Grover, A. K. Observation of tunable exchange bias in Sr_2YbRuO_6. *Appl. Phys. Lett.* **97**, 182505 (2010).
21. Huang, S. et al. Magnetic exchange bias and high-temperature giant dielectric response in $SmCrO_3$ ceramics. *Ceram. Int.* **40**, 13937–13943 (2014).
22. Galkin, V. Y., Ortiz, W. A. & Fawcett, E. Strong unidirectional anisotropy in spin-density-wave $(Cr+6.5\%Co)_{1-x}V_x$ alloys. *J. Appl. Phys.* **87**, 6543–6545 (2000).
23. Yang, F. Y. & Chien, C. L. Oscillatory exchange bias due to an antiferromagnet with incommensurate spin-density waves. *Phys. Rev. Lett.* **90**, 147201 (2003).
24. Buzdin, A. I. Proximity effects in superconductor-ferromagnet heterostructures. *Rev. Mod. Phys.* **77**, 935–976 (2005).
25. Stamopoulos, D., Manios, E. & Pissas, M. Enhancement of superconductivity by exchange bias. *Phys. Rev. B* **75**, 014501 (2007).
26. Dybko, K. et al. Possible spin-triplet superconducting phase in the $La_{0.7}Sr_{0.3}MnO_3$/$YBa_2Cu_3O_7$/$La_{0.7}Sr_{0.3}MnO_3$ trilayer. *Phys. Rev. B* **80**, 144504 (2009).
27. Samal, D. & Anil Kumar, P. S. Observation of the intense de-pairing effect in $YBa_2Cu_3O_{7-\delta}$ due to the spin injection from $La_{0.5}Sr_{0.5}CoO_3$. *J. Phys. Condens. Matter* **21**, 492203 (2009).
28. Wang, J. et al. Interplay between superconductivity and ferromagnetism in crystalline nanowires. *Nat. Phys.* **6**, 389–394 (2010).
29. Nemes, N. M. et al. Exchange-bias-modulated inverse superconducting spin switch in CoO/Co/$YBa_2Cu_3O_{7-\delta}$/$La_{0.7}Ca_{0.3}MnO_3$ thin film hybrids. *Phys. Rev. B* **81**, 024512 (2010).
30. Jin, W. T. et al. Phase diagram of Eu magnetic ordering in Sn-flux-grown $Eu(Fe_{1-x}Co_x)_2As_2$ single crystals. *Phys. Rev. B* **94**, 184513 (2016).
31. Ren, Y. et al. Temperature-induced magnetization reversal in a YVO_3 single crystal. *Nature* **396**, 441–444 (1998).
32. Yin, L. H. et al. Multiple temperature-induced magnetization reversals in $SmCr_{1-x}Fe_xO_3$ system. *Mater. Res. Bull.* **48**, 4016–4021 (2013).
33. Liu, Q. et al. Magnetic properties of La doped $SmFeO_3$. *J. Magn. Magn. Mater.* **469**, 76–80 (2019).
34. Mizokawa, T., Sudayama, T. & Wakisaka, Y. Electronic structure of LaFeAsO: yz/zx orbital degeneracy and excitonic instability. *J. Phys. Soc. Jpn.* **77**, 158–159 (2008).
35. Xiao, Y. et al. Magnetic structure of $EuFe_2As_2$ determined by single-crystal neutron diffraction. *Phys. Rev. B* **80**, 174424 (2009).
36. Jiang, S. et al. Structural and magnetic phase transitions in $Ca_{0.73}La_{0.27}FeAs_2$ with electron-overdoped FeAs layers. *Phys. Rev. B* **93**, 054522 (2016).
37. Dai, P. C., Hu, J. P. & Dagotto, E. Magnetism and its microscopic origin in iron-based high-temperature superconductors. *Nat. Phys.* **8**, 709–718 (2012).
38. de la Cruz, C. et al. Magnetic order close to superconductivity in the iron-based layered $LaO_{1-x}F_xFeAs$ systems. *Nature* **453**, 899–902 (2008).
39. Tian, W. et al. Interplay of Fe and Nd magnetism in NdFeAsO single crystals. *Phys. Rev. B* **82**, 060514 (2010).
40. Iimura, S. et al. Large-moment antiferromagnetic order in overdoped high-T_c superconductor $^{154}SmFeAsO_{1-x}D_x$. *Proc. Natl Acad. Sci. USA* **114**, E4354–E4359 (2017).
41. Błachowski, A. et al. Shape of spin density wave versus temperature in AFe_2As_2 (A=Ca, Ba, Eu): a Mössbauer study. *Phys. Rev. B* **83**, 134410 (2011).
42. Bonville, P., Rullier-Albenque, F., Colson, D. & Forget, A. Incommensurate spin density wave in Co-doped $BaFe_2As_2$. *Europhys. Lett.* **89**, 67008 (2010).
43. Wang, P. et al. Coexistence of antiferromagnetic ordering and superconductivity in the $Ba(Fe_{0.961}Rh_{0.039})_2As_2$ compound studied by Mössbauer spectroscopy. *Phys. Rev. B* **84**, 024509 (2011).
44. Jin, W. T. et al. Magnetic structure of superconducting $Eu(Fe_{0.82}Co_{0.18})_2As_2$ as revealed by single-crystal neutron diffraction. *Phys. Rev. B* **88**, 214516 (2013).
45. Kotani, A. Theory of the incommensurate sinusoidal spin-density-wave in chromium and its alloys. *J. Phys. Soc. Jpn.* **38**, 974–980 (1975).
46. Pynn, R., Press, W., Shapiro, S. M. & Werner, S. A. Second and third harmonics of the spin density wave in chromium metal. *Phys. Rev. B* **13**, 295–298 (1976).
47. Kulikov, N. I. & Tugushev, V. V. Spin-density waves and itinerant antiferromagnetism in metals. *Sov. Phys. Usp.* **27**, 954–976 (1984).

48. Kresse, G. & Hafner, J. Ab initio molecular dynamics for liquid metals. *Phys. Rev. B* **47**, 558–561 (1993).
49. Kresse, G. & Furthmuller, J. Efficiency of ab-initio total energy calculations for metals and semiconductors using a plane-wave basis set. *Comp. Mater. Sci.* **6**, 15–50 (1996).
50. Kresse, G. & Furthmuller, J. Efficient iterative schemes for ab initio total-energy calculations using a plane-wave basis set. *Phys. Rev. B* **54**, 11169–11186 (1996).
51. Monkhorst, H. J. & Pack, J. D. Special points for Brillouin-zone integrations. *Phys. Rev. B* **13**, 5188–5192 (1976).

ACKNOWLEDGEMENTS

We would like to thank Xian-Xin Wu and Lv-Kuan Zou for useful discussions and thank Fan Cui for the help on the figures of the FSs. The work was supported by the National Natural Science Foundation of China (11904414, 11774402, and 11704167); National Key Research and Development Program of China (2019YFA0705702); the National Key Research Program of China (2018YFA0704200 and 2016YFA0300301); and the Fundamental Research Funds for the Central Universities (2021qntd27).

AUTHOR CONTRIBUTIONS

J.Y. conceived the ideas, contributed to most of the experiments and data processing, and led the writing. Z.R. and M.W. supervised the research and co-wrote the paper. C.L. performed the theoretical calculation and cowrote the corresponding part. Z.W.L. and B.Z. contributed to the Mössbauer spectroscopy investigation and the corresponding writing. L.L. processed the SXRD data and contributed to part of the MPMS measurements. Z.J.L. synthesized the La-doped polycrystalline samples. T.L. and B.R. performed the experiments on the Pr-doped series. B.S. contributed to part of the PPMS measurements. All authors discussed the results and contributed to the preparation of the paper.

COMPETING INTERESTS

The authors declare no competing interests.

ADDITIONAL INFORMATION

Supplementary information The online version contains supplementary material available at https://doi.org/10.1038/s41535-021-00362-1.

Correspondence and requests for materials should be addressed to J.Y., Z.R. or M.W.

Reprints and permission information is available at http://www.nature.com/reprints

Publisher's note Springer Nature remains neutral with regard to jurisdictional claims in published maps and institutional affiliations.